Design and Characterization of an Electrothermally Driven Monolithic Long-Stretch Microdrive in Compact Arrangement

Chenpeng Hsu and Wensyang Hsu

***Abstract*—An electrothermally driven long stretch microdrive (LSMD) is presented for planar rectilinear motions in hundreds of micrometers. Design concept is based on connecting several actuation units in series to form a cascaded structure to accumulate relative displacement of each unit, and two cascaded structures are further arranged in parallel by a connection bar to double output force. The proposed area-saving design features monolithic compliant structure in compact arrangement to achieve long stroke. In experiments, the maximum reversible operating voltage is 3 V. In addition, the voltage-displacement relation shows good linearity within $\pm 5\%$ in 0.5–3.0 V. Fabricated nickel LSMD can generate displacement up to 215 μm (W $=$ 8 μm, $\theta = 0.2°$, D $=$ 34 μm) at 3 dc volts (669 mW). The maximum operation temperatures of tested LSMDs at 3 V are below 300 °C. Output forces up to 495 μN are measured by *in situ* passive micromechanical test beams. The LSMD can be operated at 100 Hz without degradation on displacement. Two geometrical design parameters, bent angle and constraint bar width, are also investigated analytically and experimentally. [1396]**

***Index Terms*—Cascaded structure, electrothermal, large displacement, metal based, microactuator.**

I. Introduction

IN MICROACTUATORS, pursuing large output displacement or output force is always the research goal in MEMS area. In material aspect, smart materials such as piezoelectrics, ferromagnet, and shape memory alloys are shown to exhibit large motions with large forces [1], [2]. However, miniaturization of these smart materials into micromechanical structures is still a problem for batch microfabrication process. Recently, electrostatic and thermal actuators made by a wide variety of materials are preferred candidates for integration of electronic circuits and microtransducers. However, single microactuator usually could provide limited output force and displacement. Coupling micromechanisms and integrating of several microactuators become an attractive way to magnify the outputs. Leverage mechanisms based on elastic linkages and hinges have shown to successfully magnify displacements [3]–[5]. However, those micromechanisms usually require large area to implement large amplification of displacements. On the other hand, microactuators connected in cascade structure could magnify displacements but not output forces [6]–[11]. Inversely, large forces can be obtained by connecting microactuators in parallel, such as comb drive with parallel capacitors [12], [13].

In this work, an electrothermally driven long stretch microdrive (LSMD) is proposed to generate continuous rectilinear planar motion for long travel range. Comparing to previous in-plane microactuators, the proposed microdrives are promising to provide large displacement (over 100 μm) at IC-level driving voltage (below 4 V) with compact device size (less than 2200 μm $\times$ 450 μm). The LSMD comprises two cascaded structures connected in parallel to double output force. Long displacements are effectively achieved by accumulating relative displacements of cascaded actuation units in each cascade structure. The monolithic device is suitable for batch fabrication and the compliant micromechanical structures prevent friction and wear. Thermal mechanical behaviors and transient thermal response are analyzed by finite-element method and investigated experimentally.

II. Concept Design

Large output displacements of the proposed microdrive are achieved by connecting several actuation units in series to form a cascaded structure that could accumulate relative displacement of each unit. Two cascaded structures are further arranged in parallel by a connection bar and hence total output force can be doubled, as shown in Fig. 1(a), where five actuation units are connected in each cascaded structure. The actuation unit is formed by two oppositely arranged actuation V-shape bent beams with a constraint bar, as shown in Fig. 1(b), where geometrical parameters are also defined. Width, bent angle, and span of the actuation bent beam, are denoted respectively as W, θ and L. D is the width of constraint bar. By applying electrical potentials across anchor 1 and anchor 2 to form a close loop, all actuation bent beams subjected to joule heating will deflect toward direction of bent angles due to thermal expansion. Each actuation unit is then stretching outward as shown in Fig. 1(b). The relative displacements delivered by all actuation units are effectively accumulated in cascaded structures to generate long stroke. Generally, more actuation units in cascaded structures can effectively magnify the output displacements of the microdrive. The key limitation comes from the fabrication capability to avoid stiction.

Manuscript received August 10, 2004; revised July 7, 2005. This work was supported by the National Science Council of the Republic of China under Grant NSC91-2212-E009-036. This work was presented in part at the 12th IEEE International Conference on Solid-State Sensors, Actuators and Microsystems Conference (Transducers'03), Session 2B3 "Large Displacement Actuators", pp. 348–351. Subject Editor N. C. Tien.

C. Hsu is with the Opto-Electronics and Systems Laboratories, Industrial Technology Research Institute, Chutung, Hsinchu, Taiwan, R.O.C.

W. Hsu is with the National Chiao Tung University, Department of Mechanical Engineering, Hsinchu, Taiwan 30010, R.O.C. (e-mail: whsu@mail.nctu.edu.tw).

Digital Object Identifier 10.1109/JMEMS.2005.859104

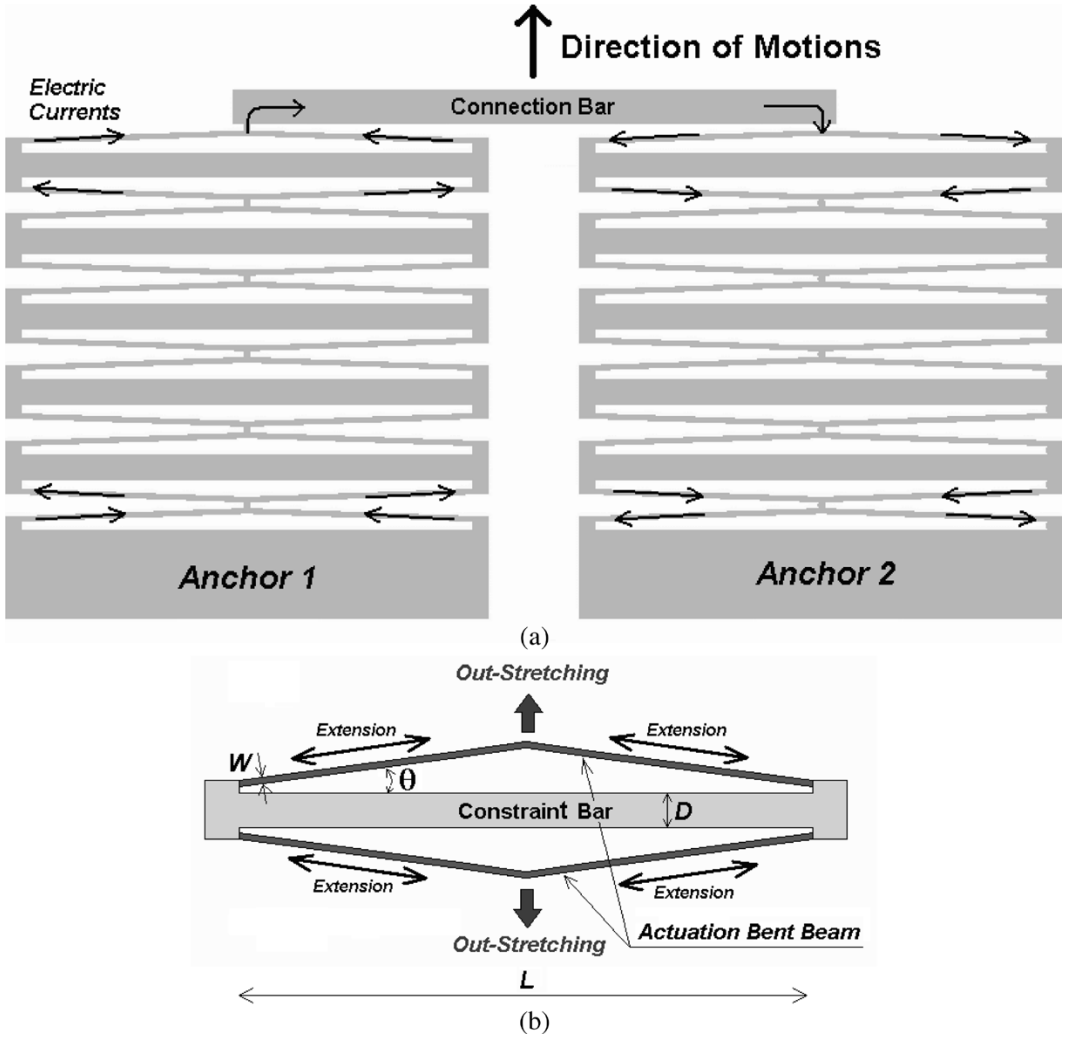

Fig. 1. (a) Concept design of the proposed LSMD with five actuation units in each cascaded structure ($N = 5$). (b) The basic actuation unit and geometrical parameter definitions.

It should be noted that the design of constraint bar is critical in output magnification. The constraint bar is used to reduce the movement at two ends of actuation bent beams, since the movement at two ends of actuation bent beam will degrade the output displacement directly. The constraint bar is not intended to have electric current flowing through in design. Therefore, the temperature rise of the bar primarily comes from the heat conduction by actuation beams. The temperature differences between constraint bar and actuation bent beam should be large to have large displacement of each beam. In addition, the mechanical strength of constraint bar should be considered in design to resist bending moments acting at its ends. Hence the constraint bar should be wide to increase the difference in temperature and mechanical strength.

III. Finite-Element Modeling

The temperature distribution and apex-deflection of a single V-shape bent-beam actuator can be evaluated by one-dimensional analysis [8], [14]. However, the proposed microdrive comprises five actuation units in each cascaded structure with eleven bent-beam actuators and five constraint bars. Every actuation bent beams will undergo different temperature risings. Furthermore, constraint bars will consume thermal energy through heat conduction that affects not only heat transfer analysis but also output displacement. Consequently, two-dimensional heat transfer analysis is preferable to estimate the longitudinal and transverse temperature profiles of the microdrive.

Instead of complicated two-dimensional analysis, finite-element simulations are conducted by commercial software ANSYS 5.5 to investigate the thermal mechanical behaviors of LSMD. Sequential two-step coupled-field analysis is used in simulation, first is the nonlinear electrothermal analysis with 3-D Solid69 element and followed by nonlinear thermal stress analysis with 3-D Solid45 element. Since the device is symmetric, the finite-element model is built in half for computational efficiency, as shown in Fig. 2. The device is made of nickel and fully surrounded by air and a silicon dioxide spacer is built beneath the electrical contact pad.

In electro-thermal analysis, reference temperature is set to be 20 °C on bottom surface of silicon substrate. Electric potential loads are applied on the top surface of the contact pad and

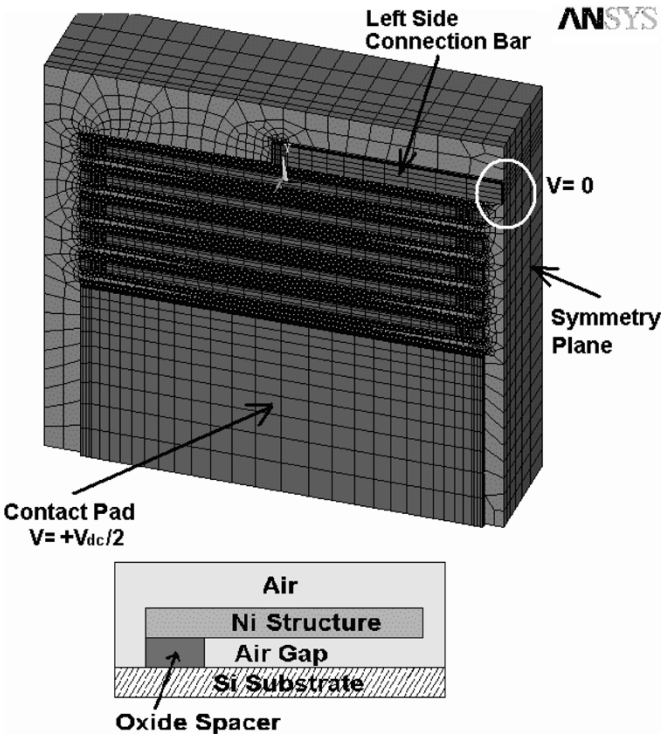

Fig. 2. Finite-element model in half-symmetry used in simulation. Where the elements of air are not shown.

on symmetry plane of the connection bar. Only conductive heat transfer mode is considered in analysis. Most of heat generated in actuation bent beams will be transferred through contact pad and air gap to the silicon substrate by conduction. Thermal conductivity and specific heat of air are temperature-dependent that can significantly alter the simulated temperature results and profiles [15]. The heat loss by free convection is related to the material, geometry and temperature of the structure, and the temperature of the surrounding medium [16]–[18]. In addition, nickel structure might be degraded at temperature higher than 350 °C [8]. Therefore, thermal convection is not considered here for simplicity, and the model is applicable to the maximum temperature of 300 °C in analysis. Beyond 300 °C, the deviations of simulated and measured maximum temperatures are becoming large which is addressed in the Section V. Hence thermal radiation effect can be neglected [17], [18].

In thermal stress analysis, temperature loads solved from electrothermal analysis are applied to nickel device structure. Large deformation effect and stress stiffening are considered in analyzes. Material properties of electrodeposited nickel depend on the deposition process, however related research is still not available. Therefore, material properties of bulk nickel are adopted and the CTE (coefficients of thermal expansion) of nickel are temperature dependent in simulation [19]. Table I lists the material properties used in simulation [8], [19]–[21].

Fig. 3(a) shows the simulated output displacement and force of the LSMD with various thicknesses at 3 V. The output force is obtained by finding the required external force to hold the connection bar of microdrive stationary at 3 V. At constant voltage, thicker device requires larger electric current to heat up actuation beams that result in higher operation temperature. Generally, thick device exhibits longer displacement and larger output force. In simulation, the 10-μm-thick nickel LSMD with five actuation units in each cascaded structure can exert forces near 400 μN at 3 V.

Fig. 4 displays the effect of air gap on output displacement. The temperature profiles of LSMD are influenced by air gap significantly. From simulation, larger air gap conducts less heat to the substrate and results in higher operation temperature. However, larger air gap causes thermal accumulation in constraint bar that depresses output displacement. Therefore, an optimum air gap of about 8 μm is found in simulation, which shows longest output displacement.

IV. Fabrication Process

Materials with large CTEs are preferable to thermal actuators. For materials commonly used in IC technology, metals such as Al, Cu, Ni, and Au have CTEs larger than 10×10^{-6} /K. Therefore, metal thermal actuators could exert larger displacements than convectional silicon-based thermal actuators under the same operation temperature. Process for deposition of thick metal film is also required to fabricate the microdrive with high mechanical strength to avoid stiction in releasing-drying process and in-use condition and to overcome out-of-plane buckling or deformations of the structure. In addition, thick microactuator delivers larger output force at lower driving voltage. Here the LSMD is fabricated by metal-based surface micromachining combing thick photoresist lithography and nickel electrofroming process, which provides thick metal structures with large CTE in high deposition rate. Besides, electroforming technique is a low temperature process (typically 40–70 °C for nickel plating), which is good for integration of monolithic transducers with integrated circuits [22].

Fabrication process requires only one mask as illustrated in Fig. 5. Due to limitation of the equipment, a 6–7 μm thick PECVD (plasma enhanced chemical vapor deposition) TEOS-SiO_2 is deposited as electrical isolation and sacrificial layer. Then Ti/Cu (20 nm/120 nm) are sputtered as plating seed layer. The Ti layer improves adhesion of SiO_2 and Cu layers. Then, 15 μm thick novolak, positive photoresist AZP4620 (AZ 4000 series, Clariant) is spun on wafer by spin coater with a corotating cover (RC8, Karl Suss) at 900 rpm for 50 s under 24–25 °C environment temperature. Photoresist is softbaked on hotplate at 90 °C for 20 min. After exposure and development of thick photoresist, the resist mold is immersed in nickel sulfamate solution to plate nickel structure. Table II lists the composition of plating bath. Electroforming is performed at 50 ± 1 °C with current densities of 8–11 $\mathrm{mA/cm^2}$ and the distance between cathode and anode electrodes is 12 cm. Thicknesses of LSMDs in the range of 10–15 μm are fabricated. The photoresist molds are subsequently stripped in acetone and then Ti/Cu seed layers are etched away. Sacrificial SiO_2 layers are etched in pure HF (49% w.t.) solution for two minutes to release the device. The devices are then rinsing in DI water and in IPA solution and dried by hot plate at 100 °C.

TABLE I
MATERIAL PROPERTIES USED IN SIMULATION [8], [17]–[19]

	Nickel	SC-Silicon	Silicon-Dioxide	Dry-Air
E : Modulus of Elasticity (GPa)	115	162	57	-
D : Density (Kg/m^3)	9040	2420	2660	*Temperature dependent:* 1.293-0.456 (273K-773K)
CTE : Coefficient of Thermal Expansion ($10^{-6}/K$)	*Temperature dependent:* 12.7-16.8 (300K~800K)	*Temperature dependent:* 2.56-4.10 (300K~800K)	0.4	-
ν : Poisson Ratio	0.31	0.28	0.245	-
κ : Thermal Conductivity (W/mK)	90.5	*Temperature dependent:* 146.4-41.8 (300K~800K)	1.1	*Temperature dependent:* 0.024-0.056 (273K~773K)
c : Specific Heat (J/Kg-K)	443.08	706.4	176	*Temperature dependent:* 1006-1093 (273K~773K)
ρ : Resisvitity (μΩ-cm)	13.5	-	-	-
- Not used in simulation.				

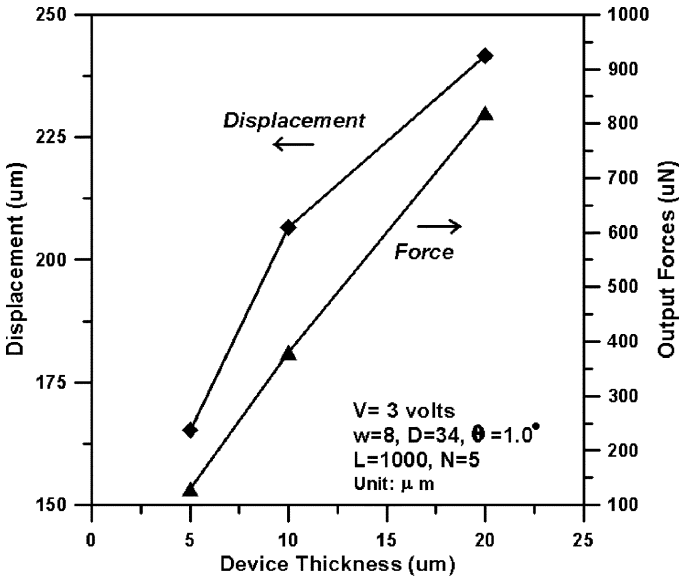

Fig. 3. Simulated output displacements and forces of the LSMDs with different structural thicknesses. ($W = 8\ \mu m$, $\theta = 1.0°$, $D = 34\ \mu m$).

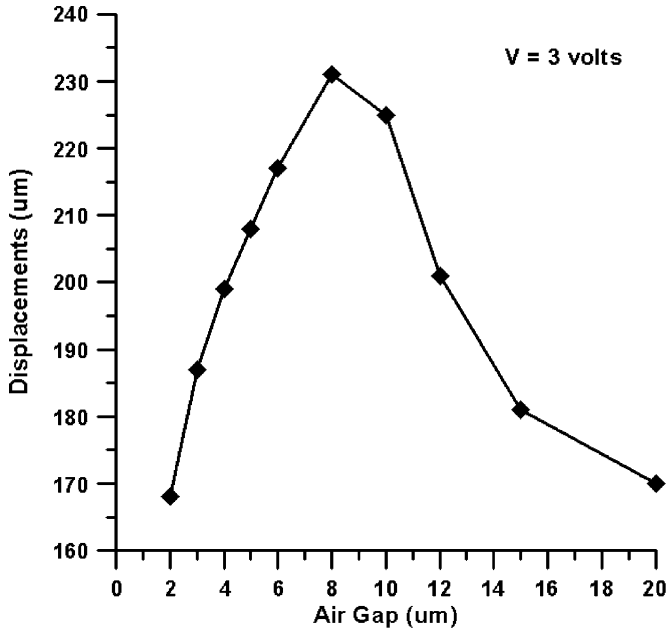

Fig. 4. The effect of air gap on output displacement. ($W = 8\ \mu m$, $\theta = 1.0°$, $D = 34\ \mu m$, thickness $= 11\ \mu m$).

V. EXPERIMENTAL RESULTS AND DISCUSSIONS

In this section, operation temperature, displacement, and output force of LSMD are characterized. Geometrical parameters, bent angle of actuation beam (θ) and width of constraint bar (D), are also investigated and discussed.

A. Operating Temperature

The temperature image of LSMD is measured by infrared thermal microscope (InfraScope II, QFI) with temperature resolution of 0.1 °C. The microscope provides automated spatial

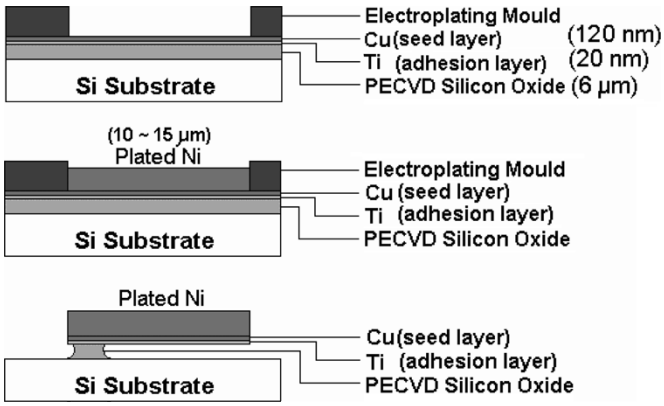

Fig. 5. One-mask fabrication process of nickel LSMD. (Metal-based surface micromachining).

TABLE II
THE COMPOSITION OF NI PLATING BATH

Composition	Quantity
Nickel Sulfamate, $Ni(SO_3NH_2)\cdot 4H_2O$	400 g/L
Nickel Chloride, $NiCl_2\cdot 6H_2O$	5 g/L
Boric Acid, H_3BO_3	40 g/L
EPC-30	10ml/L
NPA	2ml/L
Wetting Agent	5 ml/L

emissivity compensation that produces a true temperature image of the tested device and computer controlled fine focusing stage. The devices are tested on a stage with controlled reference temperature of 70 °C. The measured and simulated maximum temperatures of LSMD under various applied voltage are shown in Fig. 6. In experiments, an irreversible darkening on the surface of nickel structures occurred at applied voltage larger than 3 V. The differences between simulated and measured temperatures are becoming more evident for working temperature exceeding 300 °C. The deviation at higher temperatures may come from the disregard of the heat loss of free convection in simulations. The microdrives generate long displacements over 200 μm with maximum temperatures below 300 °C at 3 dc volts in experiments and simulations.

B. Relation of Displacement and Applied Voltage

Testing is performed on probe station with CCD camera connecting to computer to capture photo images. DC bias voltage is applied by power supply to actuate LSMD and static output displacements are measured under optical microscope. Resolution on displacement calibration is 1.5 μm. All tested devices consist five actuation units ($N = 5$) in each pair of cascaded structures where span of actuation bent beam (L) is 1000 μm. The device sizes ($\theta = 0°$–$2°$) excluding electrical contact pads are within area of 2200 μm $\times$ 450 μm.

Fig. 7 shows the pictures of nickel microdrive with dimensions of 8.0 μm bent beam width, 34 μm constraint bar width, and bent angle of 0.2° before and after actuation. Longest stretch up to 215 μm is measured for the device at 3 dc volts and 223 mA. Output performance over 200 μm/1 mm^2 (output displacement/active device area excluding electrical contact pads)

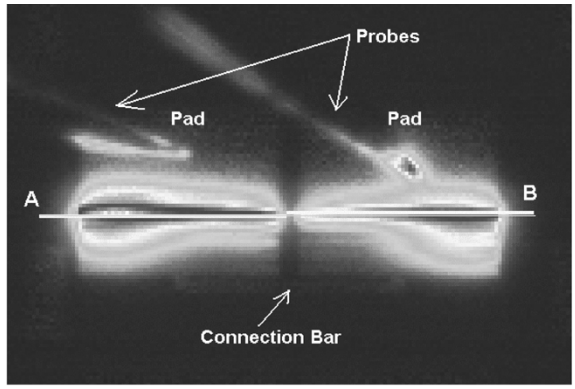

(a)

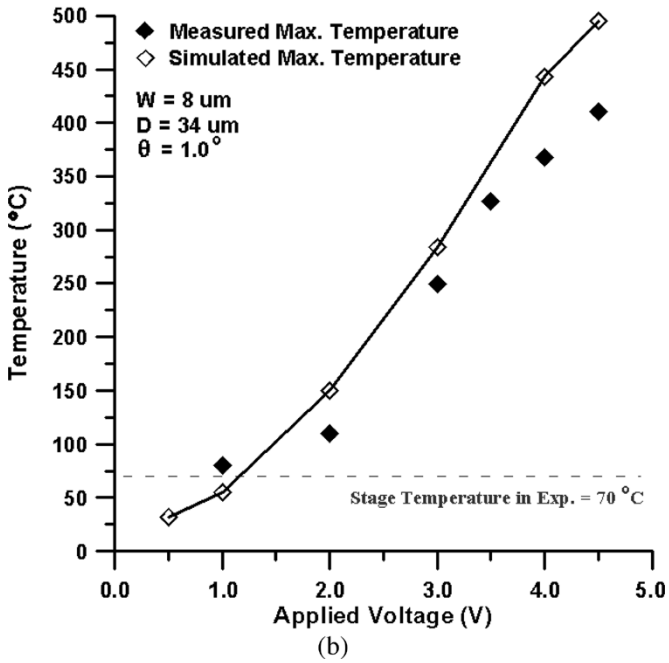

(b)

Fig. 6. (a) Measured temperature profile of LSMD. (b) The maximum temperatures of LSMD under various applied voltages. ($W = 8$ μm, $\theta = 1.0°$, $D = 34$ μm).

is achieved. It shows LSMD is a very efficient thermal actuator to exhibit long displacement up to several hundred micrometers in a compact size. The voltage-displacement relation is shown in Fig. 8. The microdrive shows good linearity within ±5% in 0.5–3.0 V. From experiment, the tested LSMD could generate displacement of about 7.8 μm per 0.1 V in 0.5–3.0 V. The maximum reversible operating voltage is 3 volt. For applied voltage larger than 3 volt, plastic deformations occur at two ends of actuation beams, which results in residual displacements of the microdrive after removing the input voltage.

However, some device exhibit rotation phenomenon due to nonsymmetrical structures on left and right units including nonuniform thickness and nonuniform line width. Hence the two cascaded structures will be subjected to different joule heating powers and stretch in different strokes. This may cause the LSMD to rotate toward the side of the cascaded structure with fewer displacements. It can be overcome by improving the electroforming process with area compensation technique to obtain uniform current density and uniform film thickness.

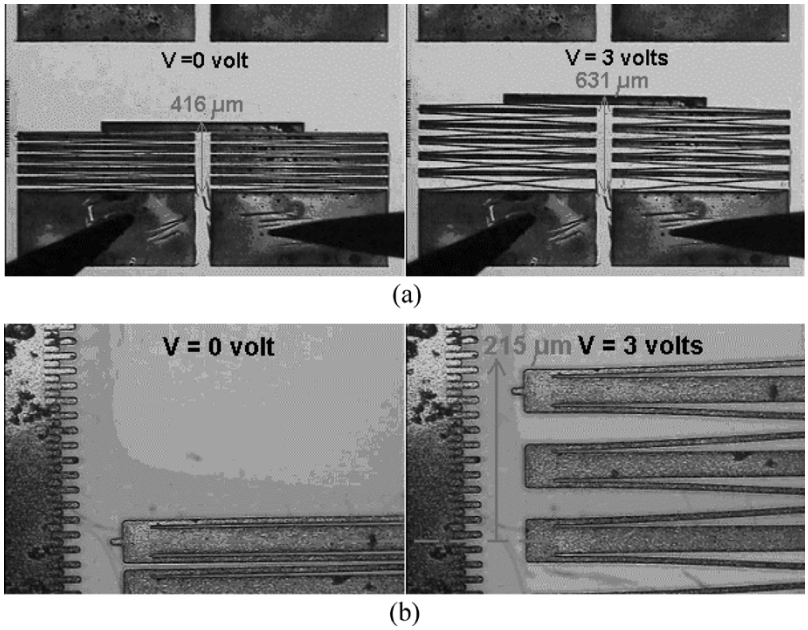

Fig. 7. Operation of the nickel LSMD which delivers stretching displacements up to 215 μm at 3 dc volts. a) Over view. b) Close-up view. The distance between fingers of indicator is 20 μm. (W = 8 μm, θ = 0.2°, D = 34 μm).

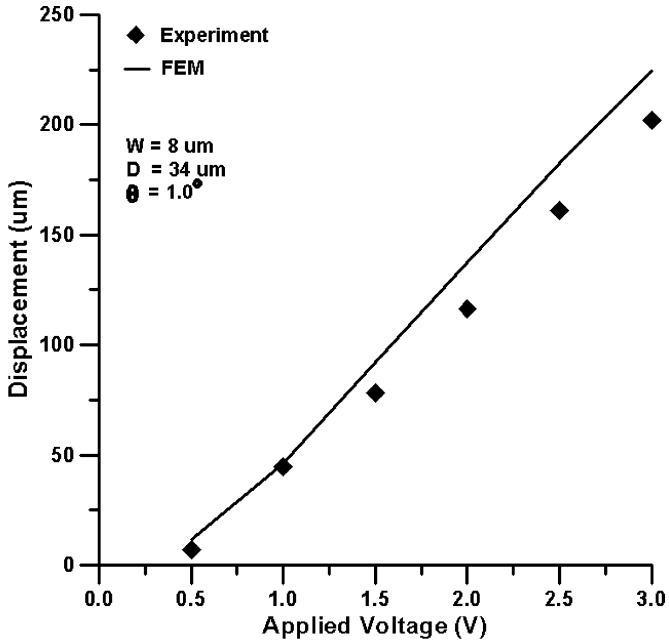

Fig. 8. Relation between displacement and applied voltage. (W = 8 μm, θ = 1.0°, D = 34 μm).

C. Output Force

Force measurement is conducted by constructing *in situ* passive micromechanical structures to interact with the LSMDs. In testing microdrive, a pair of cantilever beam arrays is located in front of the microdrive on two sides as a passive force tester. To measure the corresponding output forces under various applied voltages, the microdrives are tested with three different loading indicators, by using one, two or three cantilevers in parallel. Fig. 9 shows the microdrives to interact with three kinds of loading indicators under various applied voltages. In operation, the microdrive first stretches without any external loading by 5 μm and then it contacts with the cantilever beam arrays and pushes these beams to bend laterally up to 3 V. It is found that while applied voltage exceeding 3 V, microdrive could not push the cantilever beams any further. The bent cantilever beams even push LSMD back at 4 V. Push back comes from significantly decrease on elastic modulus of nickel at high structural temperature and the increase on compliance of the stretched cascaded structures. Therefore, the planar stiffness of LSMD is reduced at higher operating temperature that subsequently decreases output force. In addition, thermal degradation and plastic deformations of nickel structures are observed at 4 V.

The output forces are estimated by measuring the deflections of the cantilever beams and calculating the forces required to bend the beams in the same deflections. Then exerted forces of LSMD at specific output displacement can be obtained, as shown in Fig. 10. The solid curves are simulated results (device thickness used in simulation is 13.0 μm) at one, two and three dc volts respectively. The three dash curves are the fitted experiment data at three different applied voltages. In experiment, the LSMD can generate output force up to 495 μN with 16.9 μm output displacement at 3 V. Therefore, it can be estimated that blocking force (zero displacement) could exceed 500 μN at 3 V. It is observed that a sharp drop of output force occurs at 3 V. From experiments, large output forces of 400–500 μN are obtained with long output displacements up to 185 μm at 3 V. However, long stretch distance makes the cascaded structure more compliant and hence sudden out-of-plane buckling happens while the external loading from force tester exceeding the critical value. The deviation between experiments and simulations may come from the thickness variation of plated nickel microdrives (from 10.0 to 15.0 μm) and material properties used in simulation.

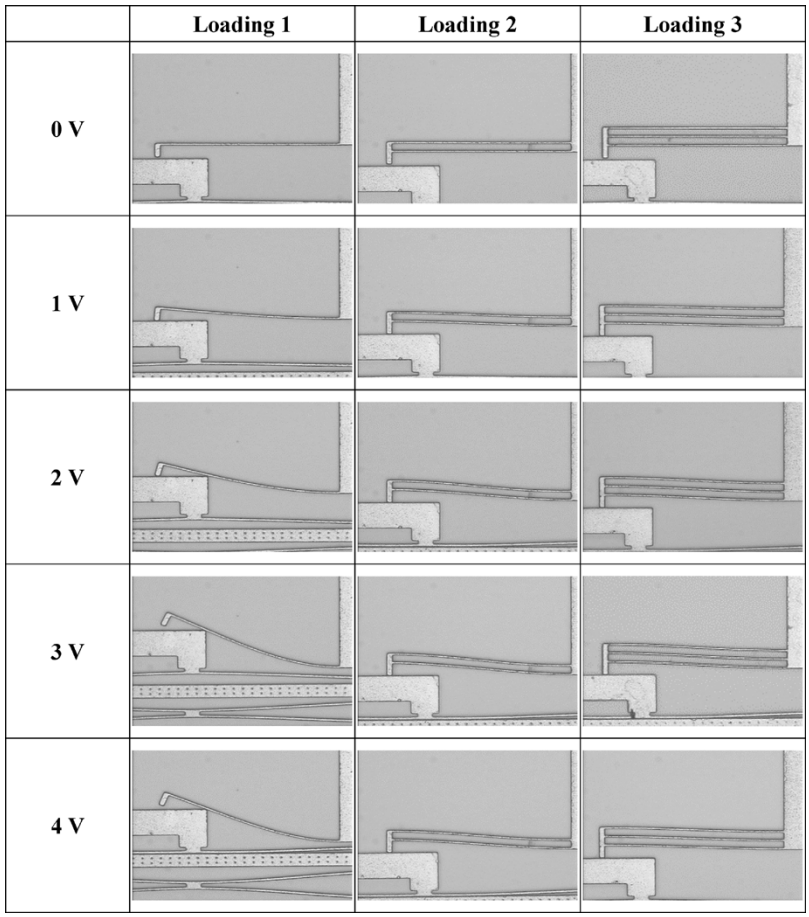

Fig. 9. The LSMDs interact with three different loading indicators at various applied voltages. (W $= 8\ \mu$m, $\theta = 1.0°$, D $= 34\ \mu$m).

D. Effects of Constraint Bar Width and Bent Angle

As mentioned in previous section, constraint bar is used to reduce the movement at two ends of actuation bent beams. Therefore, temperature rises should be small compared to the bent beams. In addition, the mechanical strength of constraint bar should be large enough to withstand the resultant bending moment acting on the ends of constraint bar. For this monolithic device, the simplest way is to increase the bar width. Fig. 11 shows the influence of constraint bar width (D) on output displacement. It is found that wide constraint bar has lower temperature rise that can enhance output displacement. However, a further wider constraint bar dissipates more thermal energy to substrate, which may reduce the output displacement resulting in limited improvement on the output displacement. For instance, increasing constraint bar width from 24 to 49 μm improves displacements by 14.5% in experiments at 3 V. Furthermore, wider constraint bar requires more device space. Hence constraint bar widths of 24–34 μm are adequate to provide large mechanical strength with acceptable thermal energy consumptions in compact arrangement. On the contrary, if the bars are too narrow, they heat up easily and have smaller temperature differences to bent beams and lower mechanical strength. For example, when bar width changes from 14 to 8 μm, output displacements are dramatically depressed in experiment where simulation indicates similar trend.

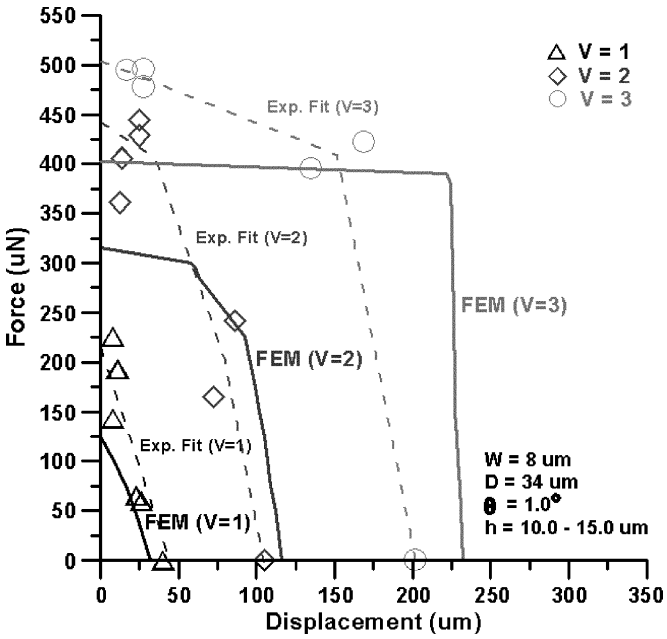

Fig. 10. Experiment and simulation results of output force versus displacement for the LSMDs at one, two, and three volts. (W $= 8\ \mu$m, $\theta = 1.0°$, D $= 34\ \mu$m, thickness $= 10.0 \sim 15.0\ \mu$m).

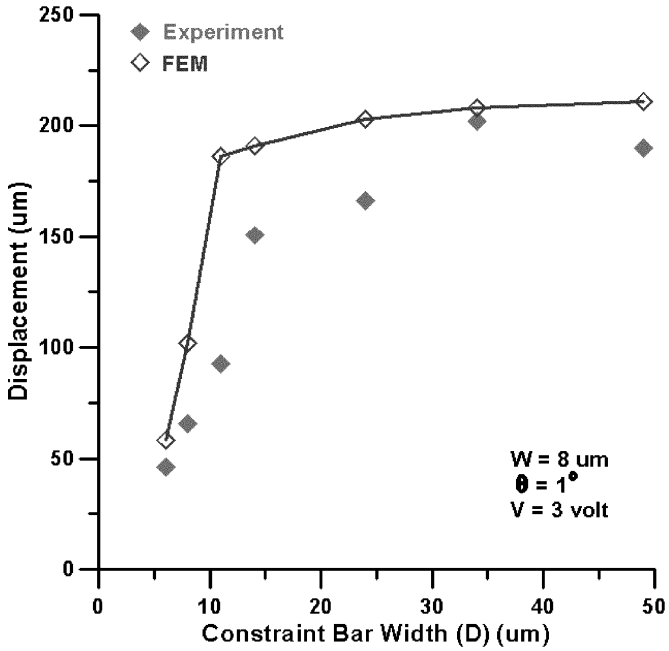

Fig. 11. Displacement versus constraint bar width of LSMD. ($\mathrm{W} = 8\ \mu\mathrm{m}$, $\theta = 1°$, $\mathrm{V} = 3$ volts).

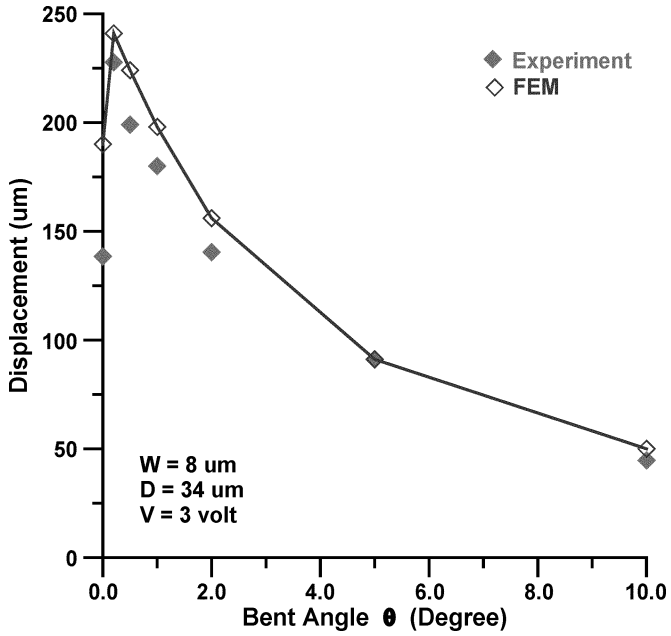

Fig. 12. Displacement versus bent angle. ($\mathrm{W} = 8\ \mu\mathrm{m}$, $\mathrm{D} = 34\ \mu\mathrm{m}$, $\mathrm{V} = 3$ V).

The bent angle of actuation beam influences the out-stretch of the actuation unit directly. Fig. 12 shows the relation of displacement and bent angle at 3 V. In general, smaller bent angle provides longer output displacement. However, if bent angle is zero, the actuation beam becomes a straight beam. The deflection directions of the straight beams are unpredictable due to thermal buckling behaviors. As shown in Fig. 13, some of actuation beams with zero angle stretch outward and some are inward at 3 V. Therefore, shrinking of each actuation unit in one or two directions may happen to depress the total output displacement of the LSMD with zero bent angles. The microdrives with bent angle of 0.2° exhibit largest displacements in experiments and simulations.

E. Dynamic Testing

In dynamic testing, the devices are observed in optical microscope with direct inspection and image capture. The devices ($\mathrm{W} = 8\,\mu\mathrm{m}, \theta = 1°, \mathrm{D} = 34\,\mu\mathrm{m}, \mathrm{V} = 3$ volts) can be operated up to 100 Hz without significant degradation in displacements. To confirm the observations in experiments, transient thermal analysis is conducted. Fig. 14 shows simulated transient (maximum) temperature response of the device under step input of 3 dc volts for 25 ms then cut-off the voltage for 25 ms. The vertical axis represents peak temperature of the device. The temperature rise time is about 10 ms that is consistent with the observation in testing. Currently, preliminary lifetime experiments conducted in air ambient indicate that LSMDs actuated at 2.5 V (50% duty cycle) can be operated over 120 000 cycles at 100 Hz without any degradation observed.

VI. Conclusion

This work has characterized the proposed electrothermal long stretch microdrive (LSMD) by finite-element analysis and experimental investigations. The structure of this monolithic device is in compact arrangement and features long displacement for several hundred micrometers in low operating voltage. Design concept is based on cascading and paralleling several actuation units. The actuation unit comprises two oppositely arranged actuation V-shape bent-beam actuators with one constraint bar. Metal-based surface micromachining is used to fabricate thick nickel structures that is preferable to thermal actuators and provides higher mechanical strength and low driving voltage (below 4 V). Fabricated nickel microdrive could generate rectilinear planar displacements up to 215 μm ($\mathrm{W} = 8\ \mu\mathrm{m}$, $\theta = 0.2°$, $\mathrm{D} = 34\ \mu\mathrm{m}$, and $2220\ \mu\mathrm{m} \times 420\ \mu\mathrm{m}$ active area) at 3 dc volts with 223 mA electrical currents (669 mW). High-output performance has been successfully achieved over 200 $\mu\mathrm{m/mm}^2$.

The voltage-displacement relation of the microdrive ($\mathrm{W} = 8\ \mu\mathrm{m}$, $\theta = 1.0°$, $\mathrm{D} = 34\ \mu\mathrm{m}$) shows good linearity within $\pm 5\%$ in 0.5–3.0 V. The operation temperatures are measured by infrared thermal microscope. The maximum temperatures of LSMD are below 300 °C at 3 V. In addition, exerting forces are measured by *in situ* method and output forces up to 495 μN are observed at 3 V with 16.9 μm displacements. Two geometrical design parameters, bent angle and constraint bar width, are also investigated. In experiments, constraint bars wider than 14 μm show better output displacements. Wider constraint bar width improves output displacement, but occupies more space. Smaller bent beam angle improves displacement significantly. However, bent angle of zero degree causes lateral buckling of actuation beam then depress output displacement. The device can be operated up to 100 Hz at 3 V without displacement degradation and transient thermal analysis sustains the observation.

In brief, the proposed electrothermal LSMD shows long displacements over 200 μm without the need to couple micromechanisms that saves substantial design area. This

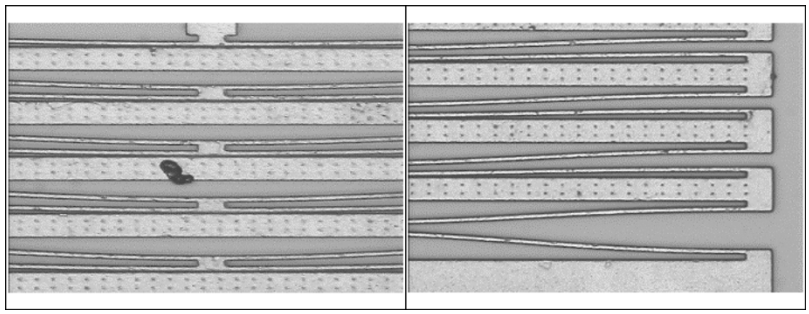

Fig. 13. Lateral buckling of actuation beams with zero bent angle, the middle portion (left photo) and the beam ends (right one). ($\mathrm{W} = 8\ \mu\mathrm{m}$, $\theta = 0°$, $\mathrm{D} = 34\ \mu\mathrm{m}$, $\mathrm{V} = 3$ volts).

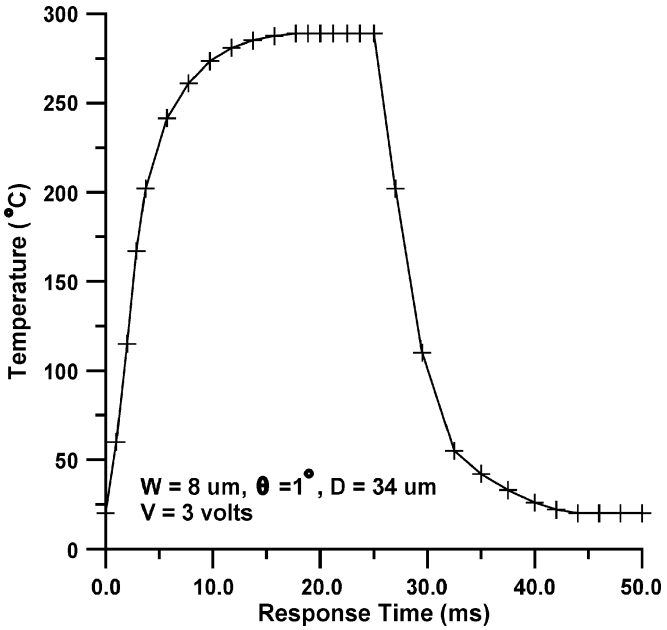

Fig. 14. Simulated (maximum) temperature response of LSMD with 50 ms duration time at 3 volts. ($\mathrm{W} = 8\ \mu\mathrm{m}$, $\theta = 0.2°$, $\mathrm{D} = 34\ \mu\mathrm{m}$).

monolithic device is suitable for low-temperature batch fabrication process on a preprocessed CMOS wafer and could be applied to tasks without high-speed requirement such as micropositioning system or microobject handling system.

ACKNOWLEDGMENT

The authors would like to thank Prof. D.-J. Yao at Institute of Microelectromechanical Systems of National Tsing Hua University for helping with the temperature measurement and the staffs of Nano Facility Center at National Chiao Tung University for providing technical support.

REFERENCES

[1] M. J. Madou, *Fundamentals of Microfabrication*, 1st ed. Boca Raton, FL: CRC Press, 1997.

[2] M. Tabib-Azar, *Microactuator*, 1st ed. New York: Kluwer Academic, 1998.

[3] L. L. Chu, J. A. Hetrick, and Y. B. Gianchandani, "High amplification compliant microtransmissions for rectilinear electrothermal actuators," *Sens. Actuators A, Phys.*, vol. 97–98, pp. 776–783, 2002.

[4] H. N. Kwon and J. H. Lee, "Characterization of micromachined inchworm motor with thermoelastic linkage actuators," in *Proc. IEEE Micro Electro Mechanical Systems Workshop*, 2002, pp. 586–589.

[5] X. T. Huang, M. T. Saif, and N. C. MacDonald, "A micromotion amplifier," in *IEEE Micro Electro Mechanical Systems Workshop*, 1996, pp. 424–428.

[6] J. W. Judy, T. Tamagawa, and D. L. Polla, "Surface micromachined linear thermal microactuator," in *Proc. IEEE*, 1990, pp. 629–632.

[7] T. Moulton and G. K. Ananthasuresh, "Micromechanical devices with embedded electro-thermal-compliant actuation," *Sens. Actuators A, Phys.*, vol. 90, pp. 38–48, 2001.

[8] L. Que, J.-S. Park, and Y. B. Gianchandani, "Bent-beam electrothermal actuators—part I: Single beam and cascaded devices," *J. Microelectromech. Syst.*, vol. 10, no. 2, pp. 247–254, 2001.

[9] J. S. Park, L. L. Chu, A. D. Oliver, and Y. B. Gianchandani, "Bent-beam electrothermal actuators—Part II: linear and rotary microengines," *J. Microelectromech. Syst.*, vol. 10, no. 2, pp. 255–262, 2001.

[10] T. Frank and C. Schilling, "The development of cascadable microdrives with muscle-like operating behavior," *J. Micromech. Microeng.*, vol. 8, pp. 222–229, 1998.

[11] T. Mineta, T. Mitsui, Y. Watanabe, S. Kobayashi, Y. Haga, and M. Esashi, "Batch fabricated flat meandering shape memory alloy actuator for active catheter," *Sens. Actuators A, Phys.*, vol. 88, pp. 112–120, 2001.

[12] M. J. Sinclair, "A high force low area MEMS thermal actuator," in *Proc. Conf. IEEE International Society on Thermal Phenomena*, 2000, pp. 127–132.

[13] W. C. Tang, T.-C. Nguyen, and R. T. Howe, "Laterally driven polysilicon resonant microstructures," *Sens. Actuators A, Phys.*, vol. 20, pp. 25–32, 1989.

[14] R. Hickey, D. Sameoto, T. Hubbard, and M. Kujath, "Time and frequency response of two-arm micromachined thermal actuators," *J. Micromech. Microeng.*, vol. 13, pp. 40–46, 2003.

[15] C. D. Lott, T. W. McLain, J. N. Hard, and L. L. Howell, "Modeling the thermal behavior of a surface-micromachined linear-displacement thermomechanical microactuator," *Sens. Actuators A, Phys.*, vol. 101, pp. 239–250, 2002.

[16] L. Lin and M. Chiao, "Electrothermal responses of lineshape microstructures," *Sens. Actuators A, Phys.*, vol. 55, pp. 35–41, 1996.

[17] M. Sulfridge, T. Saif, N. Miller, and K. O'Hara, "Optical actuation of a bistable MEMS," *J. Microelectromech. Syst.*, vol. 11, no. 5, pp. 574–583, 2002.

[18] A. A. Geisberger, N. Sarkar, M. Ellis, and G. D. Skidmore, "Electrothermal properties and modeling of polysilicon microthermal actuators," *J. Microelectromech. Syst.*, vol. 12, no. 4, pp. 513–523, 2003.

[19] *MEMS Material Database Measurement*, [Online]. Available: http://mems.isi.edu/mems/materials/, Available:

[20] J. P. Holman, *Heat Transfer*, 6th ed. New York: McGraw-Hill, 1989.

[21] J. W. Gardner, *Microsensors: Principles and Application*. : Wiley, 1994.

[22] M. Wycisk, T. Tönnesen, J. Binder, S. Michaelis, and H.-J. Timme, "Low-cost post-CMOS integration of electroplated microstructures for inertial sensing," *Sens. Actuators A, Phys.*, vol. 83, pp. 93–100, 2000.

Chenpeng Hsu received the M.S. and Ph.D. degrees in mechanical engineering from National Chiao Tung University, Taiwan, R.O.C., in 1998 and 2003, respectively.

Since 2003, he has been responsible for engineering activities including high-power lighting module and spatial-light modulators for applications of telecommunication and display in the optoelectronics modules and packaging department of Opto-Electronics and Systems Laboratories, Industrial Technology Research Institute (ITRI), Taiwan. His interests include microactuators, integration of MEMS, and CMOS for optical applications in microsystems.

Wensyang Hsu received the M.S. and Ph.D. degrees in mechanical engineering from the University of California, Berkeley, in 1990 and 1992, respectively.

He is the Professor in the Mechanical Engineering Department at the National Chiao Tung University, Taiwan. His current interests include microactuators and metal-based surface micromachining.